Interface-induced complex electronic interference structures in Ag films on Ge(111)

Y. Liu,[1,2] N. J. Speer,[1,2] S.-J. Tang,[3] T. Miller,[1,2] and T.-C. Chiang[1,2,3,4]

[1]*Department of Physics, University of Illinois at Urbana-Champaign, 1110 West Green Street, Urbana, Illinois 61801-3080, USA*

[2]*Frederick Seitz Materials Research Laboratory, University of Illinois at Urbana-Champaign, 104 South Goodwin Avenue, Urbana, Illinois 61801-2902, USA*

[3]*Department of Physics, National Tsing Hua University, 101, Section 2, Kuang-Fu Road, Hsinchu, Taiwan 30013, Republic of China*

[4]*Department of Physics, National Taiwan University, No. 1, Sec. 4, Roosevelt Road, Taipei, Taiwan 10617, Republic of China*

(Received 16 June 2008; published 29 July 2008)

We have mapped the electronic structure of atomically uniform films of Ag grown on Ge(111) by angle-resolved photoemission. Cuts in the momentum space at constant energies near the Fermi surface reveal intricate patterns resembling interfering waves emanating from multiple centers. The measured dispersion relations exhibit zigzag patterns with multiple energy gaps. These features are attributed to the mixing of electronic standing waves by the Ag-Ge interface potential as confirmed by the observed pattern symmetry and by an experimentally deduced interaction strength that scales as the inverse film thickness.

DOI: 10.1103/PhysRevB.78.035443 PACS number(s): 73.21.Fg, 73.20.At, 79.60.Dp

I. INTRODUCTION

As the thickness of a thin film approaches the electronic coherence length, quantum effects, including diffraction and interference, can become dominant influences on physical properties. This paper is a study of the emergence of complex electronic behavior in atomically uniform thin Ag films grown on Ge(111). This is a prototypical metal-semiconductor system with simple and well-understood components. The combined system, however, shows a much richer electronic structure as revealed by the three-dimensional mapping of the spectral function by the angle-resolved photoemission spectroscopy. Constant-energy contours in momentum space and energy-vs-momentum dispersion relations show a tangle of multiple intertwined bands rife with energy gaps and anticrossing features. The results can be understood in terms of the three basic effects; confinement of electrons within the film, mixing of waves by the bulk Ag crystal potential, and mixing of waves by the incommensurate interface potential. These effects separately give rise to quantum-well states in films,[1–5] band dispersions, and umklapp reflections at the interface,[6,7] respectively—each of which has been well documented. Together, they conspire to give rise to the complex phenomenon to be reported herein. In particular, the intricate Fermi surface that is far from the bulk form can be an important issue or opportunity for useful quantum transport properties and device applications of ultrathin films.

The choice of the material system employed in this study is motivated by several considerations. Ag is the best electrical conductor at room temperature and Ge is a standard electronic substrate material. Ag and Ge do not intermix or react appreciably and Ag films on Ge(111) can be grown with a thickness uniform at the atomic scale over a large area.[8] The Ag/Ge system, with a metallurgically and chemically simple metal-semiconductor interface, is of basic interest to quantum physics in confined material systems and device science at the nanoscale.

II. EXPERIMENTAL DETAILS

The experiment was performed at the Synchrotron Radiation Center, University of Wisconsin-Madison. A Ge(111) substrate was prepared by sputtering at 700 K followed by annealing at 900 K over many cycles to obtain a sharp $c(2\times 8)$ diffraction pattern. Ag films were deposited onto the substrate at 50 K and then annealed at room temperature. The resulting Ag films were oriented with the crystallographic axes parallel to the corresponding ones in the Ge substrate but the two lattices were incommensurate. We mapped the spectral function of the films at 50 K using a photoemission analyzer equipped with a two-dimensional detector that yielded dispersion relations of energy versus in-plane momentum along a selected direction.[9] A three-dimensional function $A(E,k_x,k_y)$, with A being the intensity or spectral weight, E being the energy, and k_x and k_y being the in-plane momentum components, was generated by rotating the sample in small increments over a large angular range ($\sim 50°$). The raw data covered an area extending beyond the first surface Brillouin zone in half of the momentum space. The results were symmetrized to yield the full spectral function.

III. RESULTS AND DISCUSSION

An overview of the results for a uniform film thickness of 9 atomic monolayers (MLs) is displayed in Fig. 1 by various planar cuts. On the left, two vertical cuts separated by 90°, one with in-plane momentum along $\bar{\Gamma}\bar{M}$ (x direction) and the other along $\bar{\Gamma}\bar{K}$ (y direction), reveal energy dispersion relations $E(k_x)$ and $E(k_y)$ along these high-symmetry directions. The spectral features are dominated by roughly parabolic bands centered at the zone center $\bar{\Gamma}$. These are the usual quantum-well subbands derived from the free-electron-like sp electrons in Ag.[1] Confinement of these electrons by the surface of the film and the film-substrate interface causes quantization along the z direction. The electrons form discrete states or quantum-well states at the zone center and they disperse with increasing $k_{\|}$ to form free-electron-like subbands. On closer inspection, one can see kinks in these dispersion relations. These kinks occur at the band edges of Ge and are caused by hybridization of the Ag electron wave

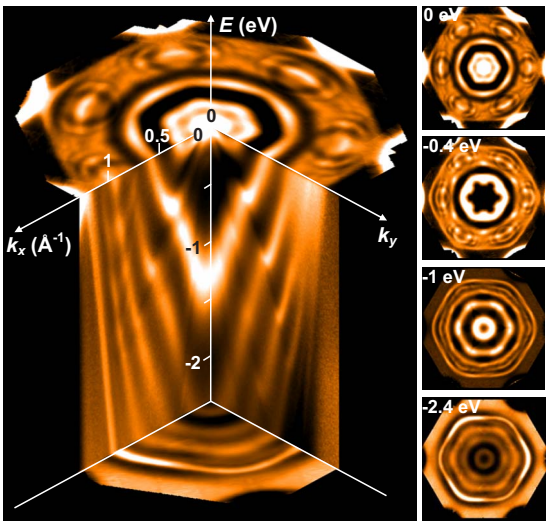

FIG. 1. (Color online) Photoemission intensities measured from an atomically uniform Ag film of 9 ML thickness on Ge(111). Various cuts of the three-dimensional data show energy-versus-momentum dispersion relations (left) and constant-energy contours (right) as labeled. The contour plots are oriented with the x axis pointing to the right and the y axis pointing upward. The photon energy used was 50 eV.

functions with those in the Ge below the band gap.[8,10] Where hybridization is allowed, the subband widths are substantially larger because the states are not fully confined. The kink and change in the band width are most obvious for the topmost valence-band edge.

In contrast to the $\bar{\Gamma}\bar{K}$ direction, the dispersion relations along the $\bar{\Gamma}\bar{M}$ direction display much richer structures near the Fermi level where the subbands develop gaps and become cross linked. The complexity is best illustrated by the constant-energy contours displayed on the right-hand side of Fig. 1. At energies far below the Fermi level (−2.4 eV), the contours are nearly circular near the zone center and become hexagonal in shape as the in-plane momentum increases. This is expected based on the standard quantum-well model; the dispersion relations of the subbands are nearly free-electron-like but are anisotropic because of the crystal potential. The contours develop six additional sets of approximately concentric-ring structures near the Fermi level as seen in the cuts at 0 and −0.4 eV. Each set of rings is centered about a $\bar{M}$ point of the Ge (not Ag) surface Brillouin zone. These six secondary sets of rings intertwine with the primary set centered at $\bar{\Gamma}$ and interference between them causes the contours to distort and vary in intensity.

A close-up of the dispersion relations near the Fermi level around the Ge $\bar{M}$ point is shown in Fig. 2(a). The same data [shown in Fig. 2(b)] are compared with calculated dispersion relations of the quantum-well subbands as indicated by the solid (cyan) curves. The calculation employed the Bohr-Sommerfeld quantization condition,[1,11]

$$(k_{1z} - k_{2z})(Nt + 2\Delta) = 2n\pi, \tag{1}$$

where k_{1z} and k_{2z} are the wave vectors of the two Bloch states—one traveling toward the surface and the other reflected from the surface, respectively—that combine to form a standing wave in the film; N is the film thickness in monolayers, t is the monolayer thickness, n is a quantum number, and Δ is the average charge spillage parameter that accounts for the finite barriers at each boundary. The band structure of Ag in this calculation was taken from an empirical model.[12] While the calculated subbands [solid (cyan) curves in Fig. 2(b)] are in good agreement with the experimental results at lower energies (below −1.5 eV), the measured spectral function is substantially more complicated at higher energies with multiple gaps in the subband dispersion relations and cross-linking segments.

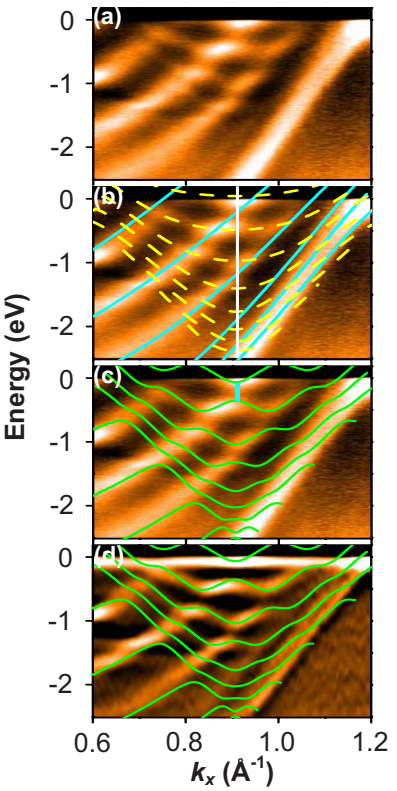

FIG. 2. (Color online) (a) Data along $\bar{\Gamma}\bar{M}$. (b) Data compared to calculated subband dispersions of the first kind (cyan/light gray solid curves) and the second kind (yellow/light gray dashed curves). The $\bar{M}$ point of Ge is indicated by a white vertical line. (c) Data compared with a model calculation (green/light gray solid curves). The cyan/light gray vertical bar indicates the size of the anticrossing gap. (d) The second derivative of the data compared with the model calculation (green/light gray solid curves).

Also shown in Fig. 2(b) (for comparison) are calculated dispersion relations of quantum-well subbands of the "second-kind" (yellow curves).[6,7] These subbands are centered at the Ge $\bar{M}$ point and are governed by the quantization condition,

$$(k_{1z} - k_{2z} + k_{3z} - k_{4z})(Nt + 2\Delta') = 2n'\pi. \tag{2}$$

These states correspond to the standing waves involving four Bloch states coupled by two specular reflections at the film surface and two umklapp reflections at the interface. The second-kind subbands can become the dominant features

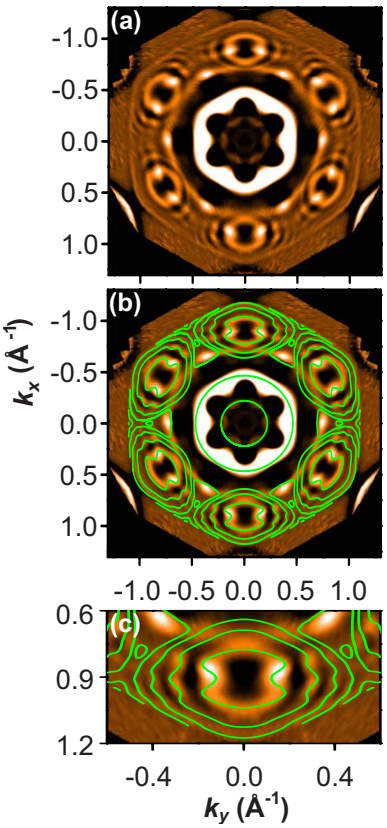

FIG. 3. (Color online) (a) Constant-energy cut at −0.4 eV through the second derivative of the three-dimensional data set. (b) The same data compared with calculation (green/light gray solid curves). (c) An enlarged view of the ring structure centered at the bottom Ge $\bar{M}$ point.

within the region of interest at larger film thicknesses or for films with lesser degrees of structural perfection. Under those conditions, contributions from the first-kind subbands diminish by a limited in-plane coherence length[13] resulting in reduced subband intertwining effects.

For the present case, the experimental results cannot be explained by these standard quantum-well pictures. The complexity is further illustrated in Fig. 2(d), in which the second derivative of the data along the energy axis is presented. The differentiation sharpens the spectral features and removes a smooth background, making it easier to follow the spectral peaks. The results show zigzag dispersion relations and multiple anticrossing energy gaps, which strongly suggest an interference coupling among the various quantum-well states.

To explain the observation in detail, we have performed a calculation incorporating the essential components of the electronic structure of the system; bulk band structure, confinement, and scattering by the interface potential. Two sets of basis wave functions are included; one set is the subband quantum-well wave functions $\psi_{n,\mathbf{k}}$ and the other set is $\psi_{n,\mathbf{k}-\mathbf{g}}$, where $\mathbf{k}$ is an arbitrary in-plane wave vector and $\mathbf{g}$ is a reciprocal-lattice vector of the Ge surface. These two sets are intermixed by the interface potential U, which has a periodicity determined by $\mathbf{g}$ and is spatially localized near the interface. The coupling matrix element

$$M_{m,n} = \langle \psi_{m,\mathbf{k}-\mathbf{g}} | U | \psi_{n,\mathbf{k}} \rangle, \tag{3}$$

is assumed to be the same for all subbands m and n over the regions of interest. The diagonal part of the Hamiltonian is constructed from the known subband dispersion relations and the off-diagonal matrix element $M \equiv M_{m,n}$ is treated as an adjustable parameter. Diagonalization of the Hamiltonian, with M set to 0.15 eV, yields the green curves in Figs. 2(c) and 2(d) where they are compared to the original data and the second derivative of the data, respectively. The observed zigzag dispersion relations and multiple energy gaps are well reproduced by the calculation. While a similar model was discussed earlier,[7] no zigzag patterns or gaps characteristic of the interference effects were observed experimentally in that work.

A much more stringent test of the above model is to compare the calculation to the three-dimensional data set at various energies. An example presented in Fig. 3(a) shows the constant-energy contours of the second-order differentiated data at −0.4 eV. The results reveal details of the six secondary sets of rings intersecting the primary set centered at $\bar{\Gamma}$. The calculated constant-energy contours are superimposed on the data in Fig. 3(b). An enlarged view of the bottom secondary ring structure is presented in Fig. 3(c) for a detailed comparison. The calculated ring shapes and positions are in excellent agreement with the experiment. Specifically, the innermost ring in Fig. 3(c) has an hourglass shape and the second ring has a number of wiggles. These subtle features are a direct consequence of the interference of the quantum-well states caused by the coupling matrix M in Eq. (3), which can be easily verified by setting M to zero in the calculation. With $M=0.15$ eV from our analysis, the anticrossing gaps are about $2M=0.3$ eV. One of the gaps in Fig. 2(c) is indicated by a vertical (cyan) bar with a height of 0.3 eV.

Since the interface potential U in Eq. (3) is limited spatially to about one atomic layer, the matrix element M is expected to scale as the inverse film thickness or $1/N$. To verify this point, we have measured the spectral function along the $\bar{\Gamma}\bar{M}$ direction for a number of different Ag film thickness. The results are summarized in Fig. 4. Here, the original data, instead of the second derivatives, are presented. Also shown are results of the same fitting analysis of the band dispersion relations as indicated by the solid (green) curves. For each case, a vertical (cyan) bar is included, which corresponds to $2M$ or the anticrossing gap. It is apparent that this gap decreases for increasing film thickness N.

The matrix element M deduced from the fits for various thicknesses is shown in Fig. 5. The curve is a fit using the functional form C/N, which describes the data well. The constant C deduced from the fit is 1.55 eV. This value within the range of typical crystal potential in solids is very reasonable. The results presented in Fig. 5 confirm that the matrix elements follow the trend expected from the model.

IV. CONCLUDING REMARKS

The essential physics of the interference pattern in this system is the coupling caused by the interface potential. In

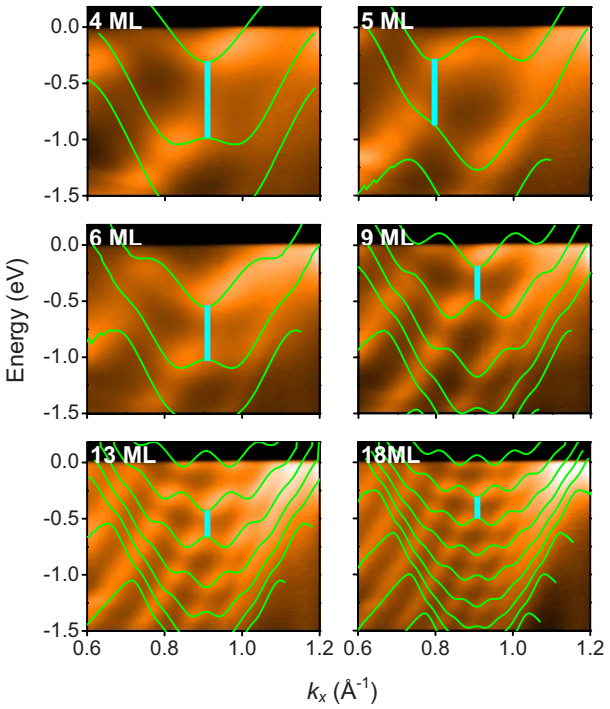

FIG. 4. (Color online) Photoemission data along $\bar{\Gamma}\bar{M}$ for N=4, 5, 6, 9, 13, and 18 ML Ag films on Ge(111). The green/light gray solid curves are fits to the band dispersions. The cyan/light gray vertical bars indicate the size of the anticrossing gap in each case.

our model, the effects of the Ag lattice and quantum confinement are included in the basis wave functions $\psi_{n,\mathbf{k}}$ and $\psi_{n,\mathbf{k}-\mathbf{g}}$ for the quantum-well states. Coupling by the incommensurate interface potential makes the system aperiodic and strictly speaking, the wave vector $\mathbf{k}$ is not a good quantum number. Nevertheless, the observed spectral function can be well described in terms of the intermixing of the basic Bloch states as demonstrated by our calculation. The case is somewhat akin to quasicrystals, which also lack spatial periodicity.[14–16]

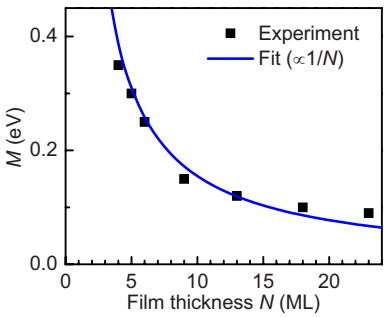

FIG. 5. (Color online) Coupling matrix element M as a function of film thickness. The curve proportional to $1/N$ is a fit.

In summary, we have observed complex electronic interference structures in atomically uniform Ag films grown on Ge(111). Thin metal films on semiconductor substrates function as miniature electron interferometers.[2] A detailed understanding of the electronic structure is important for the advancement of device concepts especially in the nanometer thickness regime. This paper shows that incommensurate scattering at the interface can cause substantial complexity in the electronic structure near the Fermi level that may in turn affect electronic transport properties. Since commensurate interfaces are few (or nonexistent), the phenomenon presented in this study is expected to be a ubiquitous feature of metal-semiconductor systems.

ACKNOWLEDGMENTS

This work was supported by the U.S. Department of Energy under Grant No. DE-FG02-07ER46383. We acknowledge the Petroleum Research Fund administered by the American Chemical Society and the U.S. National Science Foundation (Grant No. DMR-05-03323) for partial support of personnel and the beamline facilities at the Synchrotron Radiation Center. The Synchrotron Radiation Center is supported by the U.S. National Science Foundation under Grant No. DMR-05-37588.

[1] T.-C. Chiang, Surf. Sci. Rep. **39**, 181 (2000).
[2] J. J. Paggel, T. Miller, and T.-C. Chiang, Science **283**, 1709 (1999).
[3] F. J. Himpsel, J. E. Ortega, G. J. Mankey, and R. F. Willis, Adv. Phys. **47**, 511 (1998).
[4] S.-Å. Lindgren and L. Walldén, *Handbook of Surface Science*, Electronic Structure Vol. 2, edited by S. Holloway, N. V. Richardson, K. Horn, and M. Scheffler (Elsevier, Amsterdam, 2000).
[5] M. Milun, P. Pervan, and D. P. Woodruff, Rep. Prog. Phys. **65**, 99 (2002).
[6] S.-J. Tang, Y.-R. Lee, S.-L. Chang, T. Miller, and T.-C. Chiang, Phys. Rev. Lett. **96**, 216803 (2006).
[7] P. Moras, L. Ferrari, C. Spezzani, S. Gardonio, M. Ležaić, P. Mavropoulos, S. Blügel, and C. Carbone, Phys. Rev. Lett. **97**, 206802 (2006).
[8] S.-J. Tang, L. Basile, T. Miller, and T.-C. Chiang, Phys. Rev. Lett. **93**, 216804 (2004).
[9] S. Hüfner, *Photoelectron Spectroscopy*, 2nd ed. (Springer-Verlag, New York, 1996).
[10] N. J. Speer, S.-J. Tang, T. Miller, and T.-C. Chiang, Science **314**, 804 (2006).
[11] P. Czoschke, H. Hong, L. Basile, and T.-C. Chiang, Phys. Rev. B **72**, 035305 (2005).
[12] D. A. Papaconstantopoulos, *Handbook of Electronic Structure of Elemental Solids* (Plenum, New York, 1986).
[13] M. A. Mueller, T. Miller, and T.-C. Chiang, Phys. Rev. B **41**, 5214 (1990).
[14] E. Rotenberg, W. Theis, K. Horn, and P. Gille, Nature (London) **406**, 602 (2000).
[15] J. Voit, L. Perfetti, F. Zwick, H. Berger, G. Margaritondo, G. Grüner, H. Höchst, and M. Grioni, Science **290**, 501 (2000).
[16] D. Naumović, Prog. Surf. Sci. **75**, 205 (2004).